NANO LETTERS

Letter

High Density n-Si/n-TiO Core/Shell Nanowire Arrays with Enhanced Photoactivity

Yun Jeong Hwang, Akram Boukai, and Peidong Yang

Nano Lett., **2009**, 9 (1), 410-415 • DOI: 10.1021/nl8032763 • Publication Date (Web): 01 December 2008

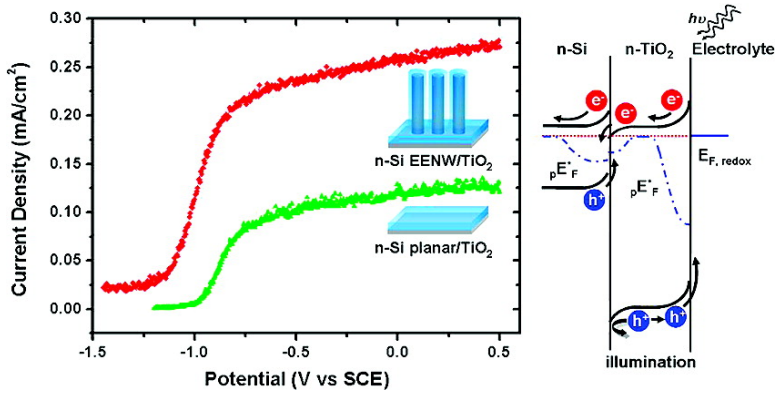

More About This Article

Additional resources and features associated with this article are available within the HTML version:

- Supporting Information
- Access to high resolution figures
- Links to articles and content related to this article
- Copyright permission to reproduce figures and/or text from this article

View the Full Text HTML

NANO LETTERS

2009
Vol. 9, No. 1
410-415

High Density n-Si/n-TiO_2 Core/Shell Nanowire Arrays with Enhanced Photoactivity

Yun Jeong Hwang, Akram Boukai, and Peidong Yang*

Department of Chemistry, University of California, Berkeley, California 94720, Material Sciences Division, Lawrence Berkeley National Laboratory, Berkeley, California 94720

Received October 30, 2008; Revised Manuscript Received November 16, 2008

ABSTRACT

There are currently great needs to develop low-cost inorganic materials that can efficiently perform solar water splitting as photoelectrolysis of water into hydrogen and oxygen has significant potential to provide clean energy. We investigate the Si/TiO_2 nanowire heterostructures to determine their potential for the photooxidation of water. We observed that highly dense Si/TiO_2 core/shell nanowire arrays enhanced the photocurrent by 2.5 times compared to planar Si/TiO_2 structure due to their low reflectance and high surface area. We also showed that n-Si/n-TiO_2 nanowire arrays exhibited a larger photocurrent and open circuit voltage than p-Si/n-TiO_2 nanowires due to a barrier at the heterojunction.

Direct solar energy conversion to storable fuels such as hydrogen offers a promising route toward less reliance on fossil fuels.[1−4] For example, photoelectrolysis of water to generate H_2 on a semiconductor/electrolyte interface has the attractive advantages of clean processing and energy savings over steam reforming of natural gas. One of the most critical issues in solar water splitting is the development of a photoanode with high efficiency and long-term durability in an aqueous environment. TiO_2 has been extensively studied as a photoanode due to its high resistance to photocorrosion.[5−10] However, its conversion efficiency of solar energy to hydrogen is still low (less than 4%)[6] due to its large bandgap (3.0∼3.2 eV). TiO_2 requires an external bias to reduce water for H_2 production to overcome the chemical over potential.[5,11] On the other hand, Si (E_g = 1.12 eV) can absorb sunlight efficiently. However, it is challenging to use Si for photoelectrolysis since it readily corrodes in water. Moreover, it is thermodynamically impossible for Si to oxidize water spontaneously due to its high valence band maximum (VBM) energy. Therefore, a composite semiconductor electrode composed of a semiconductor heterojunction has been proposed to compensate for these shortcomings. In these cases, the photoanode is composed of a small band gap semiconductor that is protected by a stable semiconductor.[12−14]

Semiconductor heterojunctions can absorb a different region of the solar spectrum.[15−18] The advantage of composite structures is that each semiconductor needs to satisfy one energetic requirement: matching the conduction band minimum (CBM) or VBM with either the H_2 reduction or O_2 oxidation potential. Single semiconductor materials typically cannot satisfy the requirements of suitable bandgap energies for efficient solar absorption and meantime with band-edges aligned with both the H_2 and O_2 redox potential of water.[3,19] Here, we prepared TiO_2 coated Si nanowire arrays and studied their photo-oxidative properties. We observed that Si/TiO_2 core/shell nanowire arrays showed higher photocurrent than the planar Si/TiO_2. A semiconductor heterojunction of n-Si/n-TiO_2 or p-Si/n-TiO_2 has different band bending properties near the junction.[12,20] The n/n heterojunction has a potential energy barrier between the two semiconductor regions that reflects minority holes in the TiO_2 similar to the back surface field in solar cell.[21] Using photocurrent and open circuit voltage measurements, we show that the n/n heterojunction is more promising for photoelectrochemical (PEC) cell application.

Highly oriented Si nanowire arrays on the silicon wafers were synthesized by an aqueous electroless etching method.[22] These Si nanowire arrays significantly suppress reflection that has the potential to provide a higher efficiency of PEC cell. We prepared n-type and p-type Si electroless etched nanowire (EENW) arrays from n-Si(100) (P doped, 0.6∼0.8 Ωcm) and p-Si(100) (B doped, 1∼5 Ωcm) wafers with dopant concentrations of ∼10^{16} cm^{-3}. A clean silicon wafer was immersed into the etching solution containing 0.04 M $AgNO_3$ (99.999%, Aldrich) and 5 M HF (49%, Honeywell) at room temperature. The length of the EENW was controlled by the etching time (0.2 μm/min growth rate).

* To whom correspondence should be addressed. E-mail: p_yang@berkeley.edu.

10.1021/nl8032763 CCC: $40.75
Published on Web 12/01/2008

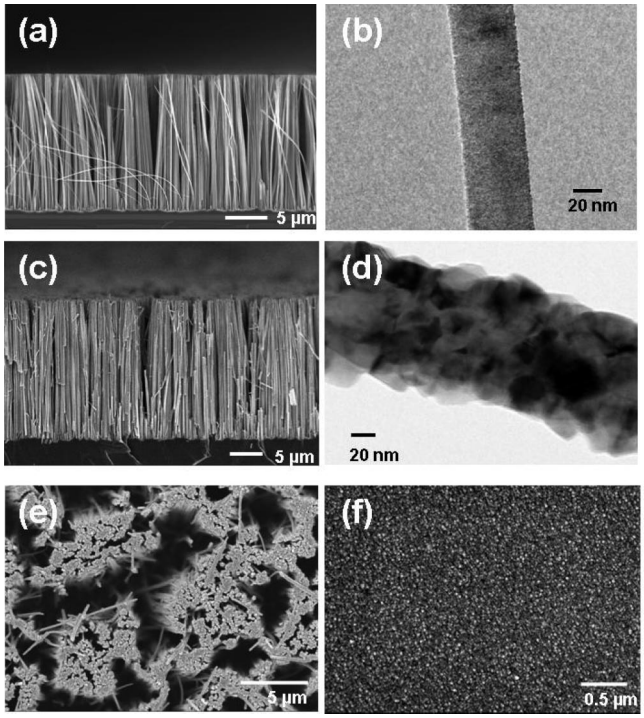

Figure 1. Characterization of Si EENW and Si/TiO_2 core/shell structures. (a) Cross-sectional SEM of 20 μm long Si EENW arrays, demonstrating vertical alignment and high density. (b) Typical TEM image of a Si EENW. (c) Cross-sectional SEM images of Si EENW arrays coated with TiO_2 by ALD at 300 °C. (d) Typical TEM image of Si EENW/TiO_2 core/shell nanowire, showing that polycrystalline TiO_2 covers the Si EENW. (e) Top view SEM images of Si EENW/TiO_2 arrays. (f) Top view SEM image of ALD grown TiO_2 thin film on a Si wafer, showing nanometer size grains of TiO_2.

TiO_2 was grown both on the Si EENW arrays and the planar Si wafer by a home-built atomic layer deposition (ALD) system with $TiCl_4$ (99.990%, Alfa) and pure water as the precursors. Si samples were cleaned with a buffered HF solution to remove the native oxide layer right before loading into the ALD vacuum chamber. The ALD system deposits polycrystalline anatase TiO_2 layer with an average growth rate of 1.2 Å per cycle on the planar Si wafer and 0.7 Å per cycle on our Si EENW arrays at 300 °C. On the Si EENW array, diffusion of the gas precursors is reduced due to the high density of the nanowire arrays, which leads to slower growth rate than the planar substrate. Care was taken to ensure that the TiO_2 thickness on the EENW arrays and planar substrates were equivalent.

Typical cross-sectional scanning electron microscope (SEM) and the transmission electron microscope (TEM) images of Si EENW and the ALD TiO_2 coated Si EENW (Si EENW/TiO_2) are shown in Figure 1a−d. The Si EENW and Si EENW/TiO_2 arrays are produced vertically on the Si wafer with high density. Si EENW maintains the same crystallinity as the starting Si wafer,[22] and their diameters are in the range of 20∼200 nm. Figure 1d shows polycrystalline TiO_2 deposition on the EENW. Figure 1e,f shows the top view SEM images of Si EENW/TiO_2 arrays and TiO_2 thin film on the Si(100) wafer with average thickness of 35 nm. The nanocrystalline nature of the TiO_2 coating is similar for deposition on the nanowire surface and on the flat wafer

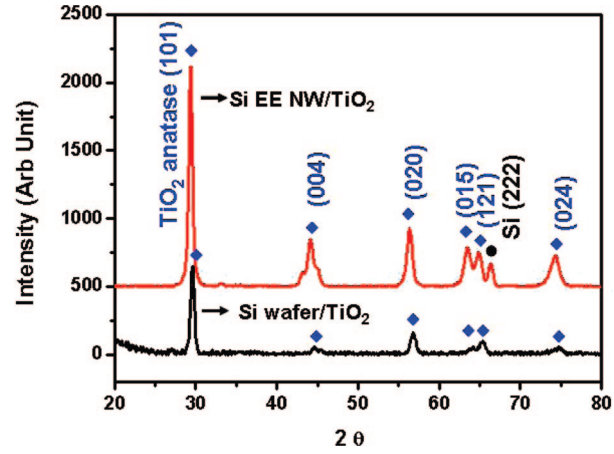

Figure 2. X-ray diffraction pattern of TiO_2 layer grown by ALD at 300 °C. 25∼40 nm TiO_2 deposited on Si EENW arrays (red line), 35 nm TiO_2 thin film on a Si planar substrate (black line). Both TiO_2 layers index to polycrystalline anatase.

surface. The X-ray diffraction (XRD) characterization indicates that the ALD grown TiO_2 layer has an anatase structure both on the Si(100) wafer and on the Si EENW array, as shown in Figure 2. For photoelectrolysis of water, anatase TiO_2 has the advantage of a flat band potential (U_{fb}) that is 200 mV more negative than that of the rutile TiO_2. This allows anatase TiO_2 to have sufficient cathodic potential for hydrogen reduction from water.[23] The carrier concentration (N_D) of TiO_2 layer by ALD was determined by capacitance versus voltage measurement. TiO_2 thin film (90 nm) was deposited on the highly doped n-Si wafer (As doped, 0.001∼0.004 Ωcm), and Ni was deposited on the TiO_2 thin film. From the Mott−Schottky relation, N_D was found to be 2.76×10^{17} cm^{-3}. The TiO_2 becomes n-type semiconductor because of defects such as oxygen vacancies and titanium interstitials, and their carrier concentration varies from $\sim 10^{17}$ to $\sim 10^{20}$ cm^{-3} depending on synthesis. [24−26]

Photocurrent measurements were performed in a 1 M KOH electrolyte with three electrodes configuration (EG&E Pinceton Applied Research Potentiostat, VersaStat II): Si/TiO_2 photoanode as a working electrode, Pt gauze as a counter electrode, and a saturated calomel electrode (SCE, Pine Research Instrumentations, AFREF1) as a reference electrode. All three electrodes are in a glass cell which has a 1 in. quartz window, and Ar gas was bubbled through to remove the dissolved oxygen during the measurement. The current versus potential measurements were carried out at a 10 mV/s sweep rate. A constant light intensity of 100mW/cm^2 from a 450 W Xe lamp (Oriel, 6266) illuminated our samples, and a liquid filter (Oriel, 6123NS) was used to avoid solution heating by infrared light.

Figure 3a shows the photocurrent versus bias potential characteristics for Si/TiO_2 composite photoanodes. Under illumination, oxidation of water takes place on the photoanode

$$4OH^- + 4h^+ \rightarrow 2H_2O + O_2 \qquad E^0 = +0.160 \text{ V (vs SCE)}$$

The photocurrent versus bias potential curves have three regions: low photocurrent density region at negative bias

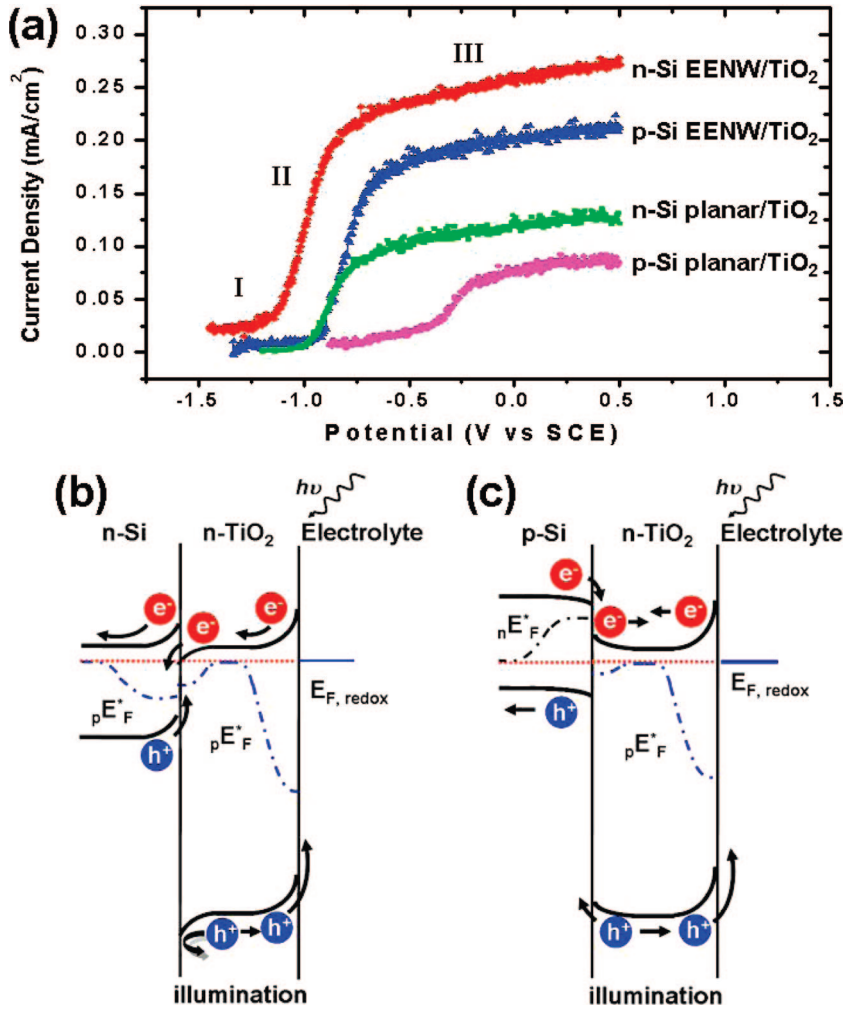

Figure 3. (a) Photocurrent density versus bias potential (vs SCE) of Si/TiO_2 photoanodes: n-Si EENW array coated by TiO_2 (red), p-Si EENW array coated by TiO_2 (blue), n-Si(100) planar substrate coated by TiO_2 (green), p-Si(100) planar substrate coated by TiO_2 (purple). Schematic representation of band energies and charge transfer (b) for n-Si/n-TiO_2 and (c) for p-Si/n-TiO_2 under the illumination. Si EENW/TiO_2 samples have 2.5 times larger photocurrent density than Si planar/TiO_2. n-Si/n-TiO_2 photoanodes have more negative onset potential than p-Si/n-TiO_2 both for planar and nanowire structures.

potential (region I), plateau of the photocurrent density at more positive bias potential (region III), and increasing photocurrent density region (region II) between regions I and III. No photocurrent passes through the semiconductor and electrolyte interface when the negative bias voltage is close to the flat band potential because any created excess holes and electrons are recombined before holes transfer into the electrolyte (region I).[27] The photocurrent plateau appears as the bias potential sweeps to more positive direction (region III), where the photocurrent is limited by the number of the holes excited by illumination.

Our planar Si/TiO_2 samples show comparable photocurrent density to those reported in the literature. The reported value[9] for a 15 μm thick film of P-25 TiO_2 on Ti foil is 0.1 mA/cm^2 under the same illumination conditions (Xe lamp, 100 mW/cm^2) even though the thickness of our ALD grown TiO_2 film is only 35 nm. At region III, 20 μm long Si EENW/TiO_2 samples show 2.5 times higher photocurrent density than planar Si/TiO_2 samples for both n-type and p-type Si. The Si EENW/TiO_2 composites have higher photocurrent mainly because of lower reflectance and larger surface area than the Si planar/TiO_2.

Figure 3a also shows that n-Si/n-TiO_2 composites have 20∼25% higher photocurrent density and more negative onset potential than those of p-Si/n-TiO_2 for both nanowire and planar structures. Higher photocurrent is expected for the n/n junction since band bending at the junction helps charge separation. The band bending of the semiconductors at the junctions are shown in Figure 3b,c. The Fermi energy (E_F) of our n and p type silicon are −4.25 and −4.97 eV (relative to the vacuum level), respectively. E_F of TiO_2 was calculated[28,29] from the reported electron effective mass in anatase ($m_e^* = 1m_e$)[30] and the measured carrier concentration ($N_D = 2.76 \times 10^{17}$ cm^{-3}). Figure 3b illustrates the charge flow in n-Si/n-TiO_2 junctions under illumination. The e^-/h^+ pairs are created inside both the Si and TiO_2 because the TiO_2 shell is transparent under visible light. Visible light can be harvested by the core Si. Under the illumination, Fermi energies of the electrons and holes, quasi-Fermi energies (E_F^*), differ from E_F in dark,[19] and the quasi Fermi

energies of minority holes ($_pE_F$*) in the n-Si and n-TiO_2 are shown. The photogenerated hole in TiO_2 ($_{TiO_2}h^+$) moves toward the n-TiO_2/electrolyte interface and oxidizes OH^- to oxygen, while photogenerated electrons in the n-TiO2 ($_{TiO_2}e^-$) move away from the front surface due to the schottky barrier at the interface with the electrolyte.

In addition to this charge separation, the interface between the n-Si and n-TiO_2 reduces the loss of holes in the TiO_2 region which results in an increase of the photoanodic current. The potential barrier seen by the holes at the n-Si/n-TiO_2 junction reflects holes back into the TiO_2 layer (Figure 3b). This is analogous to the back surface field of a solar cell which has shown larger photocurrent and larger output voltage by adding a heavily doped region adjacent to the contact.[31] To complete the circuit, the photogenerated electrons in the n-Si ($_{Si}e^-$) move to the counter electrode where the reduction reaction takes place. The photogenerated hole in n-Si ($_{Si}h^+$) moves toward the n-Si/n-TiO_2 junction and recombines with the $_{TiO_2}e^-$. Therefore, n-Si/n-TiO_2 core/shell structure shows the largest increase in photocurrent since its band alignment at the junction helps reduce recombination under illumination. In the case of p-Si/n-TiO_2 junctions, the flow of electrons and holes at the junction of p-Si/n-TiO_2 is opposite to the desirable direction. Figure 3c shows that $_{TiO_2}h^+$ can move either to the electrolyte or to the p-Si in p/n junction. Therefore, the p-Si/n-TiO_2 junction has smaller observed photoanodic current density than n-Si/n-TiO_2.

The larger photocurrent in the n-Si/n-TiO_2 leads to a larger negative onset potential. This is a result of the n/n junction's effective charge separation that leads to a larger short circuit current (J_{sc}).[31] Both n-Si EENW/TiO_2 and p-Si EENW/TiO_2 have similar dark current values (5 μA/cm^2). Also, higher V_{oc} is expected for n-Si/n-TiO_2 since the E_F and band energies of the n-Si and n-TiO_2 shift upward at open circuit under the illumination. The V_{oc} of n-Si/n-TiO_2 photoanode is $V_{oc} = V_{oc}(TiO_2/electrolyte) + V_{oc}(Si/TiO_2)$.[20] For the p-Si/n-$TiO_2$, the band energies of the n-TiO_2 shift upward but the band energies of the p-Si shift downward. The photovoltage at the p-Si/n-TiO_2 junction is in the opposite direction to the photovoltage at the n-TiO_2/electrolyte interface due to the downward band bending. The V_{oc} of p-Si/n-TiO_2 photoanode is $V_{oc} = V_{oc}(TiO_2/electrolyte) - V_{oc}(Si/TiO_2)$.

We can take the advantage of the higher V_{oc} of the n/n junction for the PEC cell. Enhanced J_{sc} and V_{oc} will provide a higher efficiency PEC cell. Also, for the solar water splitting, larger V_{oc} provides high enough cathodic potential to reduce the water to hydrogen. It is important that the flat band potential of the semiconductor is lower than the hydrogen reduction potential. For example, Fe_2O_3 ($E_g = 2.1$ eV) and WO_3 ($E_g = 2.6$ eV) have been studied due to higher stability and lower band gap than TiO_2. However, both need an external bias voltage to complete the water splitting since their CBMs are lower than hydrogen reduction potential by 0.2 and 0.1 V.[6] Therefore, the n/n composites have the potential for the spontaneous photoelectrolysis of water.

Stability is another important requirement for the PEC cell. By coating the Si with TiO_2, we can make the photoanode stable in the 1 M KOH aqueous solution. The n and p type Si EENW/TiO_2 core/shell structures have shown constant photocurrent levels while testing for one hour (Supporting Information Figure S1). In contrast, planar Si wafers and Si EENW arrays generate vigorous H_2(g) bubbles in the KOH electrolyte and as a result they are etched.

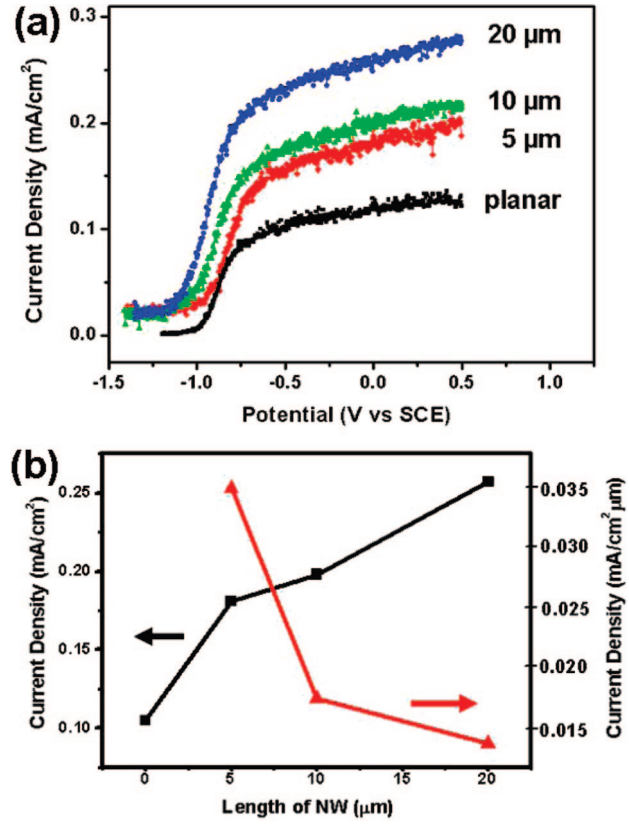

Figure 4. (a) Variation of photocurrent density versus potential depending on the length of n-Si EENW/TiO_2 arrays: 20 μm (blue line), 10 μm (green line), 5 μm (red line) long NW arrays and n-Si planar/TiO_2 (black line). (b) Relationship between photocurrent density versus the length of n-Si EENW/TiO_2, illustrating longer wire arrays have higher photocurrent. The axis to the right is the current density normalized by the length of the nanowire.

Figure 4 demonstrates the photocurrent density depending on the length of the n-Si EENW/TiO_2 arrays. We prepared 5, 10, and 20 μm long n-type Si EENW/TiO_2 arrays and planar n-Si/TiO_2. We observed that the longer Si EENW/TiO_2 arrays have higher photocurrent although the photocurrent density normalized by the length of the nanowires decrease as shown in Figure 4b. All of the three Si EENW/TiO_2 arrays had significantly lower reflectance than Si planar/TiO_2 sample (Supporting Information Figure S2). The Si EENW/TiO_2 sample can effectively trap the light by extending the path length due to multiple reflection in a high density array structures similar to textured surfaces.[32] When the wires are 5~20 μm long, their reflectance values are nearly the same. All of the three different length Si EENW/TiO_2 arrays have about 1~2% of reflectance in the UV region (200~350 nm), and about 5% of reflectance in the visible region (450 ~900 nm). In addition to low reflectance, the high surface area of Si EENW is also expected to contribute to the higher photocurrent since it increases the interface area with the

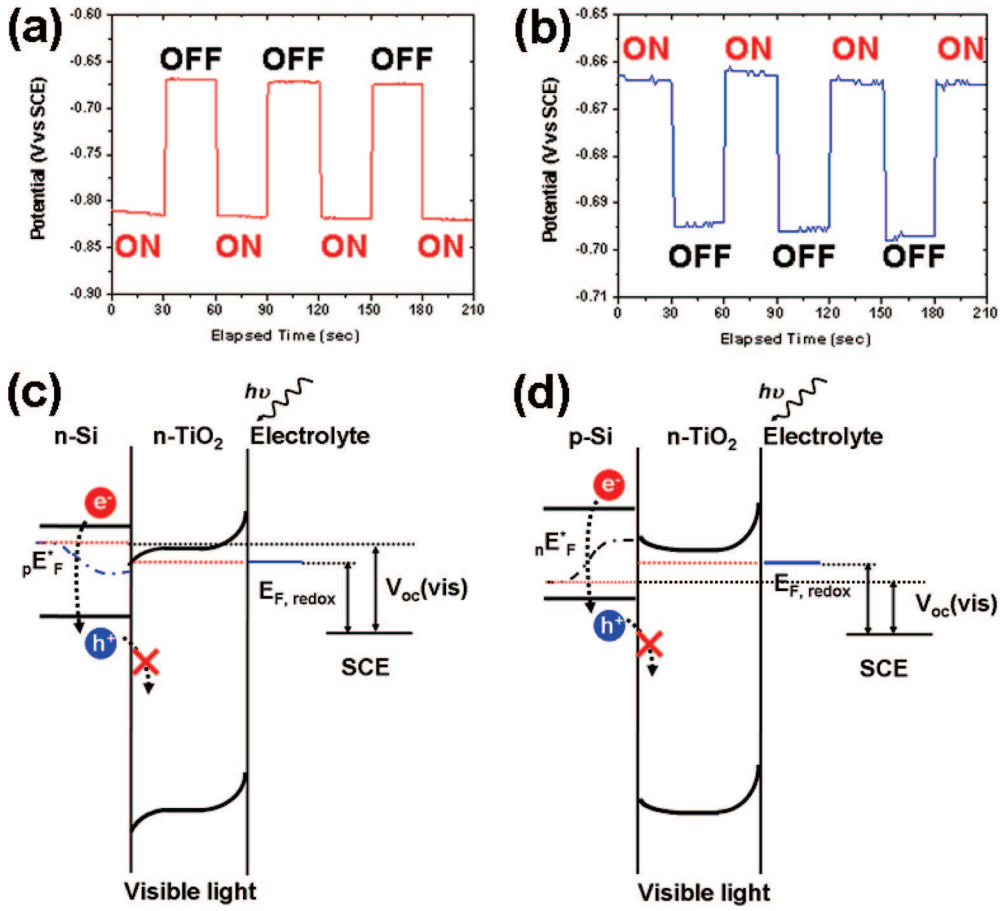

Figure 5. Open circuit voltage (V_{oc}) versus elapsed time for (a) n-Si EENW/TiO_2 and (b) p-Si EENW/TiO_2 arrays under visible light illumination only (<420 nm, ON) and in dark (OFF), and schematic diagram of band bending and V_{oc} for (c) n-Si EENW/TiO_2 and (d) p-Si EENW/TiO_2 arrays under visible light illumination, demonstrating that n-Si EENW/TiO_2 increase V_{oc} the while the p-Si EENW/TiO_2 decrease the V_{oc} under visible light.

electrolyte as well as the overall amount of TiO_2. Lower reflectance and higher surface area of the Si EENW/TiO_2 contribute to higher absorption and higher photocurrent density than the planar samples.

In order to ascertain the contribution of the core Si, we measured the photocurrent and V_{oc} of the Si/TiO_2 photoanodes under the visible light illumination only. The light was passed through a 441.6 nm edge filter to cut off the UV region from the Xe lamp so that carriers are generated only in the Si. We observed that there was no photocurrent under the visible light for all Si/TiO_2 composites. Photogenerated holes in Si cannot be transferred to the valence band of TiO_2 since there is a significant barrier at the junction (Figure 5c,d). Instead, the photogenerated e^-/h^+ pairs in the Si recombine so that there is no net charge flux.[19,33] Therefore, photo-oxidation cannot take place at the TiO_2 surface unless carriers are photogenerated in the TiO_2 shell.

The V_{oc} shifts under visible light illumination only as shown in Figure 5a,b. For n-Si/n-TiO_2, the photogenerated holes in the Si move toward the TiO_2 and recombine with electrons in TiO_2 due to an electric field in space charge region. The charge separation shifts the E_F* and the band energies of the n-Si upward, so that the space charge region diminishes. When flat band is attained, there will be no more charge separation. Therefore, the V_{oc} of the n-Si/n-TiO_2 photoanode becomes more negative (Figure 5a,c). For p-Si/n-TiO_2, the band bending of the p-Si diminishes similar to n-Si/n-TiO_2, but the reduced band bending shifts the band energies of p-Si downward which reduces the V_{oc} under visible light (Figure 5b,d). From the change of the V_{oc} under visible light, we confirmed that the core Si absorbs the visible light and it contributes shift of the band energies.

In conclusion, we compared the photocurrent density of the planar Si and Si EENW coated by ALD TiO_2 thin film. The Si EENW/TiO_2 has 2.5 times higher photocurrent density than the planar Si/TiO_2 due to lower reflectance and higher surface area. We also observed an increase of the photocurrent by using n-Si/n-TiO_2 heterojunctions because n/n junctions enhance the charge separation and minimize recombination. The n/n heterojunction is a promising structure for solar water splitting since the photovoltage at the junction can compensate the lower energy level of the conduction band of the shell semiconductor. Also, the n/n heterojunction could potentially increase the efficiency of the photovoltaic cell due to a higher open circuit voltage and higher photocurrent.

Acknowledgment. This work was supported by the Director, Office of Basic Energy Sciences, Chemical Sciences, Materials Sciences and Engineering Division, of the

U.S. Department of Energy under Contract No. DE-AC02-05CH11231. We thank Professor Nate Lewis and his group for helpful discussion and assistance in the initial testing of our samples.

Supporting Information Available: This material is available free of charge via the Internet at http://pubs.acs.org.

References

(1) Lewis, N. S.; Nocera, D. G. *Proc. Natl. Acad. Sci. U.S.A.* **2006**, *103*, 15729.
(2) Sanderson, K. *Nature* **2008**, *452*, 400.
(3) Grätzel, M. *Nature* **2001**, *414*, 338.
(4) Nowotny, J.; Sorrell, C. C.; Sheppard, L. R.; Bak, T. *Int. J. Hydrogen. Energy* **2005**, *30*, 521.
(5) Fujishima, A.; Honda, K. *Nature* **1972**, *238*, 37.
(6) Rajeshwar, K. *J. Appl. Electrochem.* **2007**, *37*, 765.
(7) Ni, M.; Leung, M. K.; Leung, D. Y.; Sumathy, K. *Renewable Sustainable Energy Rev.* **2007**, *11*, 461.
(8) Kitano, M.; Matsuoka, M.; Ueshima, M.; Anpo, M. *Appl. Catal., A* **2007**, *325*, 1.
(9) Park, J. H.; Kim, S.; Bard, A. J. *Nano. Lett.* **2005**, *6*, 24.
(10) Kongkanad, A.; Dominguez, R. M.; Kamat, P. V. *Nano. Lett.* **2007**, *7*, 676.
(11) Kavan, L.; Grätzel, M.; Gilbert, S. E.; Klemenz, C.; Scheel, H. J. *J. Am. Chem. Soc.* **1996**, *118*, 6716.
(12) Takabayashi, S.; Nakamura, R.; Nakato, Y. *J. Photochem. Photobiol. A* **2004**, *166*, 107.
(13) Morisaki, H.; Watanabe, T.; Iwase, M.; Yazawa, K. *Appl. Phys. Lett.* **1976**, *29*, 338.
(14) Lin, C. Y.; Fang, Y. K.; Kuo, C. H.; Chen, S. F.; Lin, C.; Chou, T. H.; Lee, Y.; Lin, J.; Hwang, S. *Appl. Surf. Sci.* **2006**, *253*, 898.
(15) Khaselev, O.; Turner, J. A. *Science* **1998**, *280*, 425.
(16) Yin, Y.; Jin, Z.; Hou, F. *Nanotechnology* **2007**, *18*, 495608.
(17) Yu, Z. G.; Pryor, C. E.; Lau, W. H.; Berding, M. A.; MacQueen, D. B. *J. Phys. Chem. B.* **2005**, *109*, 22913.
(18) Mor, G. K.; Vargnese, O. K.; Wilke, R. H.; Sharma, S.; Shankar, K.; Latempa, T.; Choi, K.; Grimes, C. A. *Nano. Lett.* **2008**, *8*, 3555.
(19) Gerischer, H. *Solar Energy Conversion*; Springer Berlin: Heidelberg, 1979; p 115−172.
(20) Wagner, S.; Shay, J. L. *Appl. Phys. Lett.* **1977**, *31*, 446.
(21) Hovel, H. J.; Woodall, J. M. *J. Electrochem. Soc.* **1973**, *120*, 1246.
(22) Peng, K. Q.; Xu, Y.; Wu, Y.; Yan, Y. J.; Lee, S. T.; Zhu, J. *Small* **2005**, *1*, 1062.
(23) Radecka, M.; Rekas, M.; Trenczeck-Zajac, A.; Zakrzewska, K. *J. Power. Sources.* **2008**, *181*, 46.
(24) Mahajan, V. K.; Misra, M.; Raja, K. S.; Mohapatra, S. K. *J. Phys. D: Appl. Phys.* **2008**, *41*, 125307.
(25) Akiknsa, Jun.; Khan, S. U. *Int. J. Hydrogen Energy* **1997**, *22*, 875.
(26) Cheng, H.; Lee, W.; Hsu, C.; Hon, M.; Huang, C. *Electrochem. Solid-State. Lett.* **2008**, *11*, D81.
(27) Bard, A. J.; Faulkner, L. R. *Electrochemical Methods: Fundamentals and Applications*; John Wiley & Sons, Inc.: New York, 1980; p 637.
(28) Bak, T.; Nowotny, J.; Rekas, M.; Sorrell, C. C. *Int. J. Hydrogen Energy* **2002**, *27*, 991.
(29) Perego, M.; Seguini, G.; Scarel, G.; Fanciulli, M.; Wallrapp, F. *J. Appl. Phys.* **2008**, *103*, 43509.
(30) Asahi, R.; Taga, Y.; Mannstadt, W.; Freeman, A. *J. Phys. Rev. B.* **2000**, *61*, 7459.
(31) Sze, S. M. *Physics of Semiconductor Devices*; John Wiley & Sons, Inc.: New York, 1981; p 790−825.
(32) Nelson, J. *The Physics of Solar Cell*; Imperial College Press.: London, 2002; p 276.
(33) Hinckley, S.; Mccann, J. F.; Haneman, D. *Sol. Cells* **1986**, *17*, 317.

NL8032763